

# Experimental Limits on Primordial Black Hole Dark Matter from the First Two Years of Kepler Data

Kim Griest, Agnieszka M. Cieplak

*Department of Physics, University of California, San Diego, CA 92093*

Matthew J. Lehner

*Institute of Astronomy and Astrophysics, Academia Sinica. P.O. Box 23-141, Taipei 106, Taiwan*

*Department of Physics and Astronomy, University of Pennsylvania, Philadelphia, PA 19104*

*Draft: 3 June 2013*

## ABSTRACT

We present the analysis on our new limits of the dark matter (DM) halo consisting of primordial black holes (PBHs) or massive compact halo objects (MACHOs). We present a search of the first two years of publicly available Kepler mission data for potential signatures of gravitational microlensing caused by these objects, as well as an extensive analysis of the astrophysical sources of background error. These include variable stars, flare events, and comets or asteroids which are moving through the Kepler field. We discuss the potential of detecting comets using the Kepler lightcurves, presenting measurements of two known comets and one unidentified object, most likely an asteroid or comet. After removing the background events with statistical cuts, we find no microlensing candidates. We therefore present our Monte Carlo efficiency calculation in order to constrain the PBH DM with masses in the range of  $2 \times 10^{-9} M_{\odot}$  to  $10^{-7} M_{\odot}$ . We find that PBHs in this mass range cannot make up the entirety of the DM, thus closing a full order of magnitude in the allowed mass range for PBH DM.

*Subject headings:* Black hole physics - Gravitational lensing: micro - dark matter

## 1. Introduction

The nature of the dark matter (DM) remains one of the most important unsolved problems in science (Feng 2010 and references therein). We know that it has a universal density around 5 times larger than that of material made of ordinary atoms, and is an essential ingredient of the current consensus cosmological model (Ade, et al. 2013), but have little information as to its actual nature. Hundreds of candidates have been proposed, with the most popular being various candidates from beyond the standard model of particle physics, many involving the lightest supersymmetric particle (LSP). Besides the thousands of theoretical papers on Supersymmetric (SUSY) weakly interacting massive particle (WIMP) candidates, there have been many experimental searches for

these DM candidates (Feng 2010). Despite some tantalizing hints, currently there seems to be no compelling WIMP candidate, SUSY or otherwise. The lack of detection of SUSY partners of any sort from the recent Large Hadron Collider (LHC) run is especially disappointing in this regard (Charchyan et al. 2012; ATLAS Collaboration 2013; CMS Collaboration 2013). SUSY has been so popular over the past few decades because it seemed to simultaneously solve the hierarchy fine-tuning problem (Martin 2011) and give a “natural” DM candidate. If SUSY partners existed below the TeV scale then the LSP annihilation cross section tended to be in the range which gave the measured relic abundance of LSP particles (Jungman et al. 1996). This so-called WIMP miracle motivated much theoretical and experimental work on

SUSY DM. The discovery of the Higgs Boson with a mass around 126 GeV (Aad, et al. 2013; Chatrchyan et al. 2013), along with the lack of SUSY particles below the TeV scale removes some of this motivation. The LSP can still be the DM, but now some fine-tuning will be required to arrive at the measured relic abundance.

More generally, we note that the theoretical and experimental emphasis on the admittedly elegant SUSY models over the past few decades may have been misplaced. Many important experimental discoveries have not verified our aesthetic desire for simple unified models. In fact, experimental breakthroughs have led us in almost the opposite direction. The discovery of cosmic microwave background (CMB) anisotropies points strongly towards an epoch of cosmic inflation in the early universe, most likely caused by a (finely tuned) inflaton scalar field. The discovery of the dark energy points to an extremely finely-tuned cosmological constant, or quintessence-like scalar field. (Even a cosmological constant can be thought of as the vacuum expectation value of a scalar field). Finally, the Higgs Boson mass of around 126 GeV (Aad, et al. 2013; Chatrchyan et al. 2013) seems to require some fine tuning.

Thus, perhaps we should abandon our Occam's razor proclivities and accept that finely-tuned scalar fields seem to be part of modern physics and thus may also be part of the solution to the DM problem. If so, then primordial black holes (PBH) should be seriously considered as DM candidates.

In light of the above, PBH DM has several things going for it. First it is one of the few standard model DM candidates. No need for SUSY or superstring inspired Grand Unified Models. The DM problem is detected primarily through gravity, so PBH DM would be a gravitational solution to a gravitational problem. There are many ways to create PBH DM, and many of these involved finely-tuned scalar fields. In the past, this has been taken as a negative for PBH DM, but the above considerations may allow rethinking of this attitude. For example, there are several double inflation models where one inflation solves the flatness, etc. problems that inflation is invoked to solve and the other inflationary epoch gives rise to PBHs (Frampton, et al. 2010; Kawasaki, Sugiyama, & Yanagida 1998) which can

then become the dark matter. Recall that one of the initial motivations for the scale-free Harrison-Zeldovich spectrum of primordial fluctuations was to avoid creating PBHs. Thus PBHs can easily be made via a tilted spectrum of fluctuations or through production of particles that then create the black holes (BH).

Note that some mechanisms of PBH creation result in a broad spectrum of PBH masses, but that double inflation mechanisms tend to create a nearly delta-function spectrum with the masses strongly concentrated near the mass enclosed in the horizon at the epoch of formation. Also note that there have been dozens of other suggested ways to create PBH DM (see, for example, Khlopov 2008; Frampton, et al. 2010; Carr, et al. 2010). Finally note that if PBHs are created early enough and in appropriate mass ranges they can evade big bang nucleosynthesis (BBN) and CMB constraints and make up the entirety of the DM.

## 2. Gravitational Microlensing of Kepler Satellite Data

Since the work of Paczynski (1986) gravitational microlensing has been used as a powerful method to probe the DM in the Milky Way. If the DM is composed of massive compact halo objects (MACHOs), its signature could be detected through the occasional magnification of stellar flux, when the objects pass near the line-of-sight to a star, as they move through the Milky Way halo. Many theoretical and experimental results have been obtained which together have eliminated MACHO DM (which includes PBH DM) in the mass range from  $3 \times 10^{-8} M_{\odot}$  to  $30 M_{\odot}$  from being the entirety of the DM (Carr, et al. 2010; Tisserand, et al. 2007; Alcock, et al. 2001, Alcock, et al. 1998; Alcock, et al. 1996; Griest 1991). The strongest limits above on MACHO DM come from observing programs toward the Large Magellanic Cloud, but here we follow Griest, et al. 2011 (Paper I) and Cieplak & Griest, 2013 (Paper II) in using microlensing of the nearby Kepler mission source stars to search for potential MACHO DM signatures. First constraints of PBH DM are being presented in Griest, et al. 2013. Here, we present a full-scale analysis of these constraints, including a more extensive study of the background sources of error. Throughout this paper we follow the meth-

ods developed by the authors mentioned above.

The Kepler telescope has a 1 m aperture with a  $115 \text{ deg}^2$  field-of-view and is in an Earth trailing heliocentric orbit (see Koch et al. (2010) and Borucki, et al. (2010) for a description of the Kepler mission). It takes photometric measurements of around 150,000 stars every 30 minutes towards the Cygnus-Lyra region of the sky. The telescope was launched in March 2009. The main goal of the Kepler mission is to discover extra-solar planets by the transit technique. For well aligned systems, a planet will cross in front of the stellar limb and cause the measured stellar flux to drop by a small amount. In order to detect Earth size planets, Kepler has exquisite photometric accuracy, measuring fluxes to one part in 10,000 or better. In this paper we analyze these same stellar lightcurves, but look instead for short duration increases in stellar flux caused by gravitational microlensing of a PBH as it passes near the line-of-sight of the star.

Naively, the nearby Kepler source stars should not be very useful for microlensing, since they are at a typical distance of 1 kpc and only 150,000 in number. In general, the sensitivity of microlensing searches for dark matter is proportional to the distance to the stars, the number of stars monitored, and the duration of the observing program (Paczynski 1986). Previous microlensing searches for DM towards the Large Magellanic Cloud (Alcock, et al. 2000; Tisserand et al. 2007) monitored more than 12 million stars at a distance of 50 kpc for 8 years, naively giving a factor of several thousand larger sensitivity than the Kepler source stars. However, as shown in Papers I and II, the finite size of the Kepler stars coupled with Kepler’s high precision photometry imply that Kepler is more sensitive than any previous microlensing experiment for PBHs in the mass range  $2 \times 10^{-10} M_{\odot}$  to  $2 \times 10^{-6} M_{\odot}$ .

### 3. Data Analysis and Event Selection

Here we present a preliminary analysis of 2 years of publicly available Kepler data (quarters 2 through 9) (<http://archive.stsci.edu/kepler>, 2013; Fraquelli & Thompson 2011);

Each quarter, the Kepler team releases around 150,000 lightcurve files each containing around 4400 flux measurements taken over about 90 days,

with a cadence of around 30 minutes (more precisely: 29.425 minutes). The data we use consists of the reported time of each flux measurement (**time**), the photometric flux (**pdccflux**), the flux error (**pdccfluxerr**), and the quality flag (**sapquality**). We use the Kepler pipeline flux data **pdccflux** which removes various trends from the data. The aperture photometry fluxes are also available but we do not use these. Since the Kepler team is looking for dips in the flux which last only a few hours and we are looking for microlensing bumps in the data which last a similarly short time, the detrending procedure the Kepler team applies to the data should be good for us as well. The quality flag is set non-zero if problems exist in the photometry, for example cosmic rays, reaction wheel desaturation, etc. (Fraquelli & Thompson 2011). We ignore all data where the quality flag is non-zero.

We divide the good fluxes by the mean flux of the lightcurve, which is calculated over 300 data points towards the center of the lightcurve, and subtract unity from this quantity to produce a fractional magnification lightcurve. We divide the flux errors by the mean as well to give us appropriate errors on the fractional magnifications. These lightcurves are used for our initial search, however, when performing fits to microlensing shapes, etc. we renormalize our selected lightcurves using the median flux of the whole lightcurve, which gives a more robust baseline. For each lightcurve we calculate a set of statistics that allow us to identify microlensing candidates events and also to distinguish various types of background events. These statistics and the selection criteria are listed in Table 1.

#### 3.1. Statistics and Selection Criteria

Since we are looking for very low magnification, short duration bumps in a large amount of data the main backgrounds are measurement noise and stellar variability. Our level 1 requirement is that a candidate event contain a “bump”, defined as 4 sequential flux measurements that are 3-standard deviations higher than the mean flux. (This was also the criterion applied in our theoretical papers: Paper I and Paper II.)

Naively applied, this criteria selects about 50% of all the 150,000 lightcurves. The problem is that given the extreme precision of Kepler photometry,

TABLE 1  
DEFINITIONS OF STATISTICS AND SELECTION CRITERIA

Statistic	Definition
$\langle f \rangle$	average of $f_i$ over all good measurements in lightcurve
$A_i$	$\text{flux}_i / \langle \text{flux} \rangle$
$\sigma_i$	reported error of flux normalized by average flux
bump	sequence of 4 or more contiguous fluxes with $A_i - 1 \geq 3\sigma_i$
nbump	number of bumps in lightcurve
bump1en	number of contiguous fluxes with $A_i - 1 \geq 3\sigma_i$
lag1autocorr	$\frac{1}{N} \sum_{i=1}^{i=N} ((A_i - 1)(A_{i+1} - 1))$
bumpvar	$\sum  A_i - 1  / \sigma_i$ over points under bump
leftedgevar	$\sum  A_i - 1  / \sigma_i$ over 2 bump1en points starting 6 bump1en before bump
rightedgevar	$\sum  A_i - 1  / \sigma_i$ over 2 bump1en points starting 4 bump1en after bump
dof	number of data points within 5 bump1en of peak minus number of fit parameters
mlchi2dof	$\chi^2$ of fit to microlensing shape divided by dof
fchi2dof	$\chi^2$ of fit to exponential flare shape divided by dof
chi2in	$\chi^2$ of microlensing fit for points with time, $t_i$ , such that $t_0 - 1.5\hat{t} < t_i < t_0 + 1.5\hat{t}$
chi2out	$\chi^2$ of microlensing fit for points with time, $t_i$ , such that $t_0 - 6\hat{t} < t_i < t_0 + 6\hat{t}$ , but not in chi2in
Nasy	number of points near peak time, $t_0$ , for asymmetry; larger of $1.5\lambda$ and $2\hat{t}$
asymmetry	$\sum_{N_{asy} \text{ points}}  A(t_0 - t_i) - A(t_0 + t_i)  / (\sum A(t_i) - N_{asy} A_{min})$
Selection Criterion	Purpose
$0 < \text{nbump} < 3$	remove variable stars and stars with no transient
$\text{bump1en} \geq 4$	level 1 trigger (significant bump)
$\text{bump1en} \geq 5$	remove short duration flare events
$\text{lag1autocorr} > 0.7$	remove obvious variable stars
$\text{bumpvar} > \frac{1}{2} 5.5 (\text{leftedgevar} + \text{rightedgevar})$	signal to noise cut when reported errors are non-Gaussian
$\text{edgecriterion} > 0$	remove bumps that start or end in bad data
$\text{mlchi2dof} < 0.75 \text{ fchi2dof}$	microlensing fit significantly better than flare fit
$\text{mlchi2dof} < 3.5$	microlensing fit is not too bad
$\text{asymmetry} < 0.17$	remove short duration flare events
$\text{chi2in}/\text{chi2out} < 4$	remove events where $\chi^2_{\text{dof}}$ under peak is much worse than $\chi^2_{\text{dof}}$ outside peak area

around 25% of main sequence stars and 95% of giant stars have measurable variability (Ciardi, et al. 2011). So before applying our bump selection criteria we first identify and remove “variable stars” from the data base. We call a star a “variable star” if it contains more than 2 bumps (defined above) and if the autocorrelation function of the lightcurve calculated with a lag time of one measurement (around 30 minutes) is larger than 0.7. This **lag1autocorr** statistic is a measure of how correlated one flux measurement is with the next. Since most variable stars vary on time scales much longer than 30 minutes, we expect variable stars to have a large value of this statistic. The threshold value of 0.7 is set by requiring that the simulated microlensing events we add to lightcurves to measure our detection efficiency are not removed by this cut. In general, the cut values of each selection criterion below is set as a compromise. We want to select as many of our added simulated microlensing events as possible, while still eliminating whatever background the cut is intended to remove. Thus our cuts are as loose as possible while eliminating background. All of our cuts are

listed and defined in Table 1.

Using these two criteria we find that we remove about 34% of the dwarf stars and around 91% of the giant stars from further consideration. Note that these numbers are consistent with the results of Ciardi, et al. (2011) mentioned above, whose numbers we used in Paper II for our theoretical estimate. Note that we are using the term “giant star” very roughly to mean any star with radius greater than  $3 R_\odot$ , as listed in the Kepler lightcurve file.

After eliminating variable stars our bump selection criteria gives us around 10,000 candidate events. However, the Gaussian error approximation implied by our bump criterion is not adequate, so we calculate three local measures of variability for each bump we find: **bumpvar**, which is the absolute value of fractional flux increase divided by the error averaged over the duration of the bump ( $\text{bumpvar} = \langle |A - 1| / \sigma \rangle$ ); **leftedgevar** which is the same for the region of the lightcurve that occurred just before the time of the bump, and **rightedgevar** which is the same for a small portion of the lightcurve just after the

bump occurred. We then demand that the variation during the time of the bump is 5.5 times more significant than the variation that occurred just before and after the bump. This selection criterion eliminates bumps in lightcurves caused by a sequence of very noisy measurements, where the noise is non-Gaussian, meaning the reported error-bars are not reliably determining the probability of outlier fluxes.

After applying these criteria we still find a large number of candidate bumps. Many of these bumps happen at the same time and have the same shape across a large number of lightcurves. These are most likely caused by systematic problems in the photometry coming from either instrumental problems in the Kepler satellite or the detrending software. We especially notice these systematic error bumps just before or after regions of “bad data”, areas of lightcurves which have the quality flag set. To deal with these problems we compiled ranges of dates over the 8 quarters which contained substantial numbers of similarly shaped bumps. These ranges of times are organized in a “bad data” file and are removed from all the lightcurves before calculating any statistics.

After removing the bad data, the variables, and the noise bumps as discussed above we still have around 100 candidate bumps per quarter, some still caused by noise but many caused by short term variability. Some example lightcurves are shown in Figures 1,2,3, and 4. Examination of the lightcurves show that the selected bumps come in several categories. First, there are dozens of bumps that start during periods of “bad data” and then exponentially approach the mean flux over several hours or days. To eliminate these we apply an **edgecriterion**, demanding that our best fit microlensing shape not start or end in a region of “bad data” or off the edge of the data; that is, we demand that the entire bump be contained in the good data.

Next, the largest category of bumps by far, containing a few hundred events, are lightcurves with a highly asymmetric bump that we determined is probably due to a stellar flare caused by magnetic activity in the stellar atmosphere. Examples are shown in Figure 1. To eliminate these flare events we compare two non-linear fits to each bump, the first using the expected microlensing shape given

by formulas in Cieplak & Griest (2013)<sup>1</sup> and the second using a flare event shape, which has a nearly instantaneous rise followed by an exponential drop back to the median lightcurve flux. For microlensing there are four parameters that determine the lightcurve shape:  $t_0$ , the time of peak (time of closest approach between the lens and source),  $\hat{t}$ , the duration of the event,  $A_{max}$ , the peak magnification, and  $\epsilon_{min}$ , the distance of closest approach between lens and source lines-of-sights divided by the stellar radius in the lens plane. For the flare shape, we have  $t_0$ , the peak time,  $A_{max}$ , the peak amplitude, and  $\lambda$ , the exponential decay constant. While we are assuming the rise is instantaneous and is followed by an exponential decay, the rise can occur at any time during the 30 minute Kepler flux integration. So the flux measurement immediately preceding the measured peak flux can have any value between the baseline and the peak value. Thus we add another degree-of-freedom (dof) to the flare fit which is the value of the flux at the time immediately preceding the peak time. Examples of these fits are shown in Figures 1 and 2, where we show the data as well as both the microlensing and flare fits.

In order to eliminate the flare events we then require that:  $\mathbf{mlchi2dof} < 0.75 \times \mathbf{fchi2dof}$ , where  $\mathbf{mlchi2dof}$  is the chi-squared per degree-of-freedom (dof) of the microlensing fit, and  $\mathbf{fchi2dof}$  is chi-squared per dof of the flare star fit. We fit over a region of the lightcurve up to ten times longer than the bump length, where the bump length is defined as the number of 3-sigma high flux points we used for the level 1 trigger. This selection criteria works extremely well in removing longer duration (i.e. many hour) flare events, but for candidate events lasting only a few hours does not always remove the flare event. See Figure 1 for longer duration events where the fits clearly distinguish microlensing from flaring, and the top two lightcurves in Figure 2 where both microlensing and flare fits are satisfactory due to the small number of data points in the bump. The prob-

<sup>1</sup>In fact, to speed the processing we fit only a linear limb darkened shape (Equation 11 of Paper II) and not the full microlensing lightcurve shape. For the PBH masses considered, the small size of the Einstein Ring relative to the projected size of the stellar limb means this is a good approximation. If we find good microlensing candidates we would, of course, fit with the complete microlensing profile.

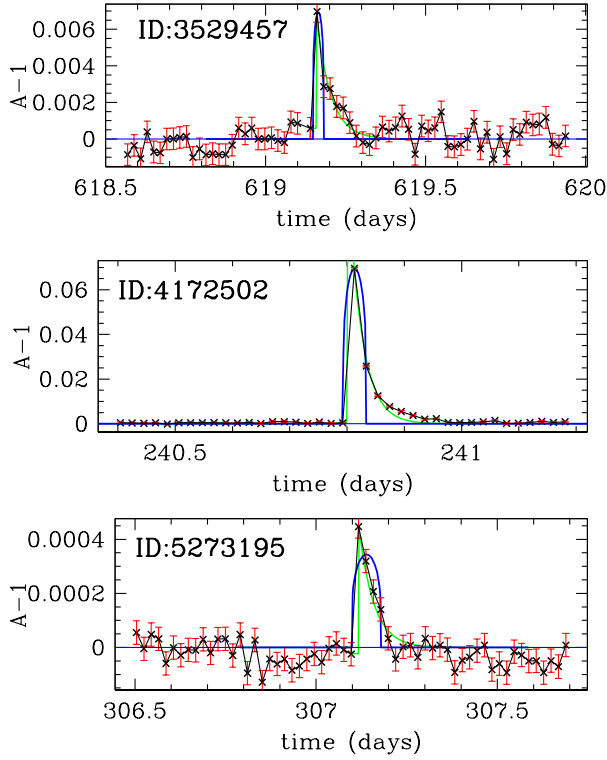


Fig. 1.— Examples of bumps in Kepler lightcurves caused by stellar flares. The Kepler source star IDs are shown in the upper left corners, the solid blue line is the rather poor fit to the microlensing shape, and the solid green line is a (better) fit to flare event. The top panel shows a medium amplitude flare event, the middle panel shows a high amplitude event, and the bottom panel shows a very low amplitude flare.

lem is that there is a large background of flare events which have a wide range of durations. We therefore expect many short duration flare events with only a few points in the bump. However, our fits lose their power to distinguish flares from microlensing when the number of data points is small. In addition, we start the fit for the flare shape from the highest point, but allow one previous flux to be high due to the roughly 30 minute Kepler integration time. Sometimes, due to measurement error, it is the third point in the flare event which is the highest and then the flare fit

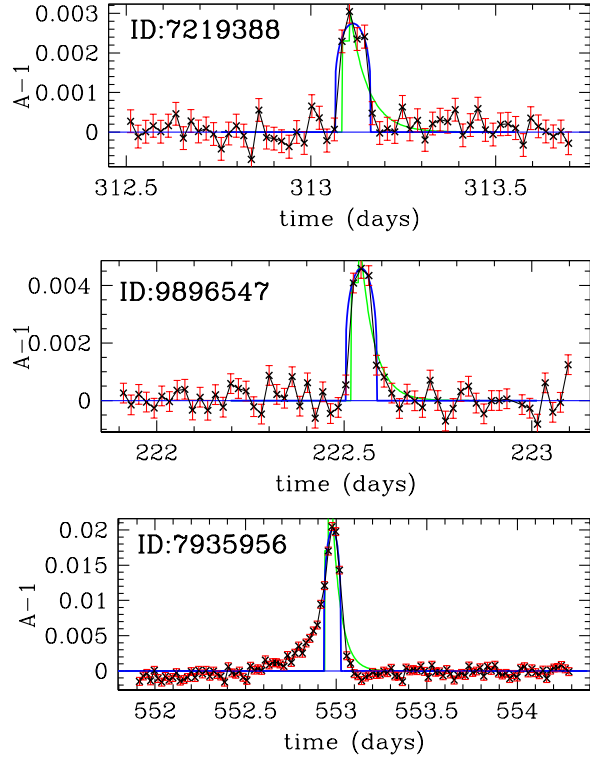


Fig. 2.— Examples of bumps in Kepler lightcurves. The top two panels show very short duration events that can be well fit with either microlensing or flare shapes. The bottom panel is an event of unknown origin that is a poor fit to the microlensing shape. The Kepler source star IDs are shown as are fits to microlensing (solid blue line) and flare (solid green line) shapes.

chi-squared is bad. With only 4 points total, there are not enough points to compensate for this one bad point and the microlensing fit will be better than the flare fit. Thus, due to random measurement errors, bumps that are near our minimum of a total of 4 flux points are sometimes fit better with a microlensing shape, even when they are probably flare events.

To solve this problem, we up our required minimum number of points from 4 to 5 sequential 3-sigma high measurements and calculate an additional asymmetry statistic, which distinguishes the symmetric microlensing shape from the asym-

metric flare shape.

To calculate **asymmetry** we start by finding a symmetry timescale which is the larger of 1.5 times the flare fit timescale  $\lambda$  and twice the microlensing timescale  $\hat{t}$ . We define **asymmetry** as the sum of absolute values of the differences between the flux measured at a time before the peak and the flux measured at the symmetric time after the peak, all normalized to the total flux above the median under the peak (See Table 1 for the formulas). Requiring that **asymmetry** be smaller than 17%, together with the above chi-squared criterion, and the new minimum number of data points effectively remove the flare events, including those of short duration.

We also implement two more signal-noise criteria, first by requiring that **mlchi2dof** (the chi-squared per degree of freedom of the microlensing fit defined above) be less than 3.5. This ensures that the microlensing shape is a relatively good fit to theory. The bottom lightcurve in Figure 2 shows an example bump removed by the chi-squared criteria. We also compare **chi2in**, the chi-squared per dof of the fit under the peak, with **chi2out**, the chi-squared per dof outside the peak. We define the a region centered on the peak of duration 3 times the event duration  $\hat{t}$  as “under the peak” and a region 6 times the peak duration that excludes the above region as “outside the peak”. Our selection criterion is to require that the ratio of **chi2in** to **chi2out** be less than 4. This selection criterion eliminates rare bumps where the extra noise in the peak area causes our bump criteria to be met. We don’t want bumps where the fit chi-squared under the peak is much worse than the chi-squared outside the peak.

### 3.1.1. Foreground Moving Objects in the Kepler field

After applying these cuts to 2 years of data we find 17 candidate microlensing events. These are listed in Table 2 and examples are shown in Figures 3 and 4.

Note that these events are nicely symmetric and reasonable fits to the microlensing (actually just stellar limb darkening) shape. However, the candidate events only occur in quarters 5 and 9, and as shown in Figure 5 occur in a pattern on the sky that makes it extremely unlikely that they are

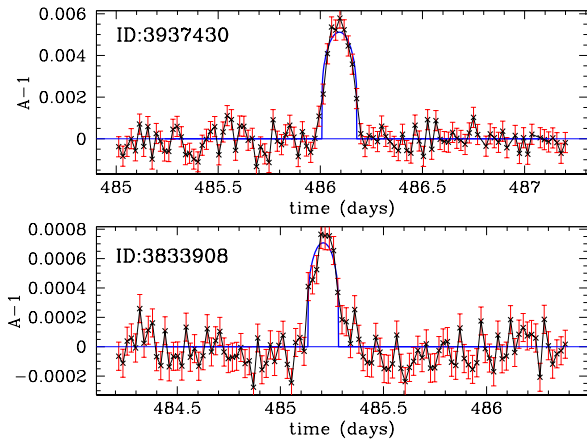


Fig. 3.— Examples of bumps in Kepler lightcurves caused by comet C/2006 Q1 (McNaught) during quarter 5. The Kepler source star IDs are shown and the solid blue line is a fit microlensing model.

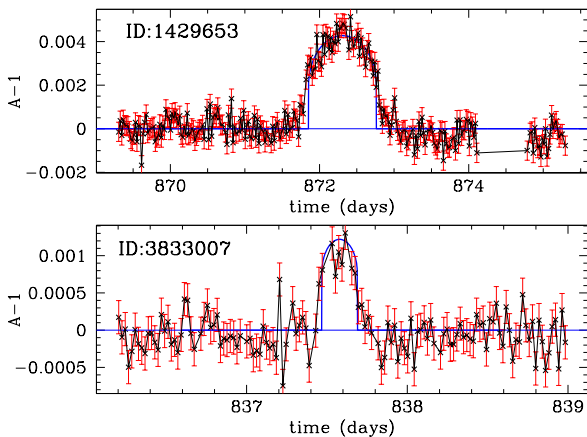


Fig. 4.— Examples of bumps in Kepler lightcurves caused by comets during quarter 9. The upper panel is from C/2007 Q3 (see Table 2) and the lower panel from an unidentified comet or asteroid. The Kepler source star IDs are shown as are fits to a microlensing shape.

due to microlensing. Considering first the quarter 5 events as shown in Figure 5 (a) and (b), we see a clear track across the Kepler field. From the times shown in Figure 5 (b) we see that an object entered the Kepler field near the lower right hand corner

(Figure 5 (a)) and moved at a constant rate to the upper left hand corner over a period of around 60 days. From the times of the bump peaks as given in Table 2, it is clear that this is an object that moved through the Kepler field leaving a track of transient brightenings in its path. Note that the probability of microlensing is so small that it is extremely unlikely that these events are all caused by microlensing by a single lens.

From the time differences between the bump peaks we deduce an angular speed of around 16 arcsec/hr. Assuming the motion is due to the 30 km/s Kepler satellite motion around the Sun, this implies a distance to this object of around 10 AU. We thus expect all these quarter 5 events to be caused by a comet passing through the Kepler field.

Using the fractional magnification from the peak flux of each event, and the  $g$  magnitude of each Kepler source star (given in the Kepler lightcurve file header), we can calculate a magnitude that needs to be added to each star to explain each bump. We find values ranging from  $g_{\text{mag}} = 20$  to  $g_{\text{mag}} = 21.5$ . The largest of these values gives a minimum magnitude of the comet.

Using the right ascension (RA) and declination (dec) of the Kepler stars and making the coordinate transformation from the Earth trailing Kepler orbit frame to the Earth frame we examine objects the using the Minor Planet Center (2013) software and find that comet C/2006 Q1 (McNaught) passed through the locations of our quarter 5 candidate events at the times they occurred. This comet was at a distance of around 10 AU, just as we estimated. Thus all these quarter 5 candidate microlensing events are consistent with being caused by comet C/2006 Q1.

Similarly examining the quarter 9 candidate events as shown in Figures 4 and 5, we see evidence for two tracks that cross the field. Using the time between bumps (Table 2) we again conclude that these events are caused by two objects moving through the Kepler field at a constant angular speed. For one of the new objects there were only 2 bumps that passed all our cuts, which does not make for much of a test for constant motion, so we loosened the cuts somewhat and found more events along this track. We show one such additional bump as a circled point in Figure 5(c) and (d). Using the positions and times we were able

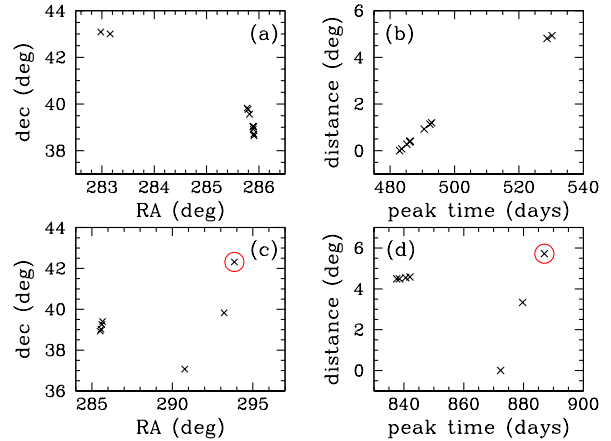


Fig. 5.— Part (a) shows right ascension (RA) and declination (dec) of bumps caused by comet C/2006 Q1 as it passed through the Kepler field during quarter 5. Part (b) shows the angular distance moved by the comet vs. Kepler time. Part (c) shows RA and dec of two separate objects moving through the field during quarter 9, and part (d) shows the distance moved by these two objects. The constant slopes in parts (b) and (d) imply a constant angular speed. The point circled is a bump that did not pass all the cuts but is shown here so there are more than two points on the line.

to identify one of these objects as comet C/2007 Q3. The other object is moving faster than the two comets and so is probably closer. We could not identify a counterpart in the Minor Planet Ephemeris (Minor Planet Center, 2013), so it may be a previously unidentified comet or asteroid. Using the same method as for C/2006 Q1 we find a minimum magnitudes of around  $g_{\text{mag}} = 21.3$  for C/2007 Q3, and  $g_{\text{mag}} = 21$  for the new bright object. In any case, we remove these events as microlensing candidates.

After removing the events due to bright moving objects from our candidate list we are left with no PBH microlensing candidates.

#### 4. Efficiency Calculation

Since we found no candidates, we can place upper limits on the halo density of PBH DM. We display these as limits on the halo fraction,



TABLE 2  
COMETS IN KEPLER DATA

quarter	Kepler ID	time <sup>a</sup>	RA <sup>b</sup>	dec <sup>b</sup>	gmag <sup>c</sup>	comet
5	3527753	482.949	285.905	38.6395	21.3	C/2006 Q1
5	3628766	483.582	285.904	38.7161	21.4	C/2006 Q1
5	3833908	485.217	285.893	38.9171	20.8	C/2006 Q1
5	3937408	486.116	285.887	39.029	21.5	C/2006 Q1
5	3937430	486.106	285.894	39.0263	21.2	C/2006 Q1
5	3937432	486.259	285.894	39.0463	21.4	C/2006 Q1
5	4447346	490.591	285.82	39.5627	21.7	C/2006 Q1
5	4637389	492.379	285.791	39.7713	22.1	C/2006 Q1
5	4729654	492.880	285.774	39.8299	21.9	C/2006 Q1
5	7421340	530.305	282.978	43.0877	20.8	C/2006 Q1
5	7421791	528.762	283.157	43.0068	20.6	C/2006 Q1
9	1429653	872.332	290.769	37.0712	21.3	new
9	3833007	837.604	285.517	38.9324	21.9	C/2007 Q3
9	3936698	838.523	285.568	39.023	21.5	C/2007 Q3
9	4138614	840.608	285.615	39.2529	21.5	C/2007 Q3
9	4347043	842.049	285.662	39.4001	22.6	C/2007 Q3
9	4751561	879.688	293.212	39.8243	21.2	new
9	6870049*	886.968	293.851	42.3156	21.9	new

<sup>a</sup>Kepler days; convert to Julian date by adding 2454833

<sup>b</sup>From the Kepler satellite point of view

<sup>c</sup>Found by adding the bump peak flux to the source star magnitude. See text.

\*Did not pass all cuts.

where a dark matter halo made entirely of PBH DM and a local density of  $\rho_{\text{DM}} = 0.3 \text{ GeV cm}^{-3}$  ( $0.0079 M_{\odot} \text{ pc}^{-3}$ ) would give a halo fraction of unity. In order to do this we need to calculate the number of microlensing events our search through the Kepler data would be expected to detect if the halo consisted entirely of PBH DM. We did this estimate previously (Paper I and Paper II), but in those theoretical analyses we made several approximations that our actual search through the data has not substantiated. For example, we assumed Gaussian errors while the actual data has many non-Gaussian excursions in flux resulting in many noise events. We did not know about the flare events or the frequency of other variability induced events. Thus we need to recalculate the expected number of detections using the actual selection criteria that gave us no PBH DM candidates. We use the same halo model as in Paper I and Paper II: a constant halo density between the Earth the Kepler field stars about 1 kpc away in a direction almost orthogonal to the Galaxy center, an isotropic Maxwellian velocity distribution, and no need for any solar motion transverse to the line-of-sight since the Sun’s rotation around the Galaxy center is in the direction of the Kepler field stars.

Using this model, we calculate the expected number of event detections by constructing simulated PBH microlensing events and adding these into actual Kepler lightcurves. We then analyze these simulated events using the same software and selection criteria that we used for our microlensing search (including, of course, removal of the “bad data” ranges of the lightcurves). To create the simulated microlensing lightcurves we use the full limb-darkened microlensing formula (Witt & Mao 1994, corrected in equation 13 of Cieplak & Griest (2013)) with linear limb darkening coefficients calculated using the Sing (2010) model grid for each Kepler source star (Paper II).

In the Monte Carlo efficiency calculation we want to cover all possible actual microlensing events, so we add simulated events covering the possible range of physical parameters. These are discussed in great detail in Papers I and II, but include  $m$ , the DM mass,  $t_0$  the time of closest approach between the lens and source lines-of-sights,  $x$ , the distance to the lens divided by the distance to the source star,  $v_t$ , the transverse speed of the lens relative to the source line-of-sight, and  $u_{\text{min}} = ux/r_E$ , distance of closest approach scaled by the Einstein radius in the lens plane. The Ein-

stein radius is given by

$$r_E = 0.0193\sqrt{x(1-x)}[(L/\text{kpc})m_9]^{1/2}R_\odot, \quad (1)$$

where  $m_9 = (m/10^{-9}M_\odot)$  and  $L$  is the source star distance.

Each time a simulated event is detected we calculate the differential microlensing rate for the microlensing parameters used, and for that specific source star, using Equation 19 of Cieplak & Griest (2013):

$$\frac{d\Gamma}{dxdu_{\min}dv_t} = 4r_E(x)L\frac{\rho}{M}\frac{v_t^2}{v_c^2}e^{-v_t^2/v_c^2}. \quad (2)$$

where  $v_c = 220\text{km/s}$  is the assumed circular speed around the Milky Way at the Sun's position. Note,  $v_c$  sets the dispersion in the assumed isotropic Maxwellian velocity distribution of the dark matter halo.

One weakness in the above calculation is our estimate of the source star distance. The header of each Kepler lightcurve file contains the stellar radius,  $R_*$ , Sloan  $r$  and  $g$  magnitudes, effective temperature,  $T_{\text{eff}}$ , star position (RA and dec), extinction parameters  $A_V$  and  $E(B - V)$ , etc. We estimate the apparent visual magnitude from:

$$V = g - 0.0026 - 0.533(g - r) \quad (3)$$

(Fukugita, et al. 1996), and the stellar distance from:

$$L \approx 1.19 \times 10^{-3} R_* (T_{\text{eff}}/T_\odot)^2 10^{0.2(V-A_V+B.C.)} \text{kpc}, \quad (4)$$

where B.C. is the bolometric correction. Note that we make a crude bolometric correction, using only the effective temperature and whether the source is a main sequence or giant star (Carroll & Ostlie 2007), but we include it because it slightly reduces the distances to the sources, thereby reducing the expected detection rate, and we want our calculation to be conservative.

By adding many millions of simulated events covering the entire allowed range of microlensing parameters we effectively perform the efficiency weighted integral over the above differential rate (Equation 2), where  $\Gamma$  is in units of expected events per day per star. By multiplying this by the number of non-variable stars and the duration of the lightcurves we thus find the efficiency-corrected number of expected microlensing events.

The number of non-variable stars and star-days for each Kepler quarter is given in Table 3.

Since we detected no events, a 95% C.L. upper limit of  $3/N_{\text{exp}}$  can be set on the halo fraction. This is similar to the method used previously by the MACHO collaboration (Alcock, et al. 1996) to set limits on low mass MACHO DM. Since the number density of PBHs, the efficiency, and the differential rate all depend strongly on the assumed PBH mass, we perform this Monte Carlo calculation independently for each value of PBH mass. Also, since each quarter of Kepler lightcurve data includes somewhat different source stars and has different noise characteristics we also calculate the expected number of events independently for each quarter and sum the total to find our limits. All together we analyzed more than 500 million simulated events. Our results are plotted in Figure 6.

## 5. Limits on PBD Dark Matter and Discussion

The thick black solid line in Figure 6 shows our new limits on the possibility of PBH DM. Since these limits depend only on the mass (assuming the lens is a compact object) they apply to any massive compact halo object, so are robust limits on planets, non-topological solitons, etc. Our analysis shows that PBH DM with masses in the range  $2 \times 10^{-9}M_\odot$  to  $10^{-7}M_\odot$  cannot make up the entirety of the dark matter in a canonical DM halo.

Also shown in Figure 6 is a black dashed line which shows the best previous limits from a combined MACHO-EROS analysis in 1998 (Alcock, et al. 1998). Note some authors (e.g. Carr, et al. 2010) only quote the 2007 EROS-only limits (Tisserand, et al. 2007) but these are not as strong as the earlier combined limits. We see that our new limits rule out more than one order of magnitude more of the allowed PBH DM mass range, for the first time eliminating masses between  $2 \times 10^{-9}M_\odot$  and  $3 \times 10^{-8}M_\odot$  as being the entirety of the DM.

Also shown in Figure 6 as a blue dot-dash line are the potential theoretical limits from analysis of the entire 8-years of Kepler data from Paper II. Naively we would have expected our limits to be about 1/4 of these theoretical limits since we analyzed 2 years of data, about 1/4 of the total

TABLE 3  
STAR-DAYS BY KEPLER QUARTER

quarter	total stars	non-variable stars	start time <sup>a</sup>	end time <sup>a</sup>	duration (days)	star-days
2	152238	94758	169.765	258.467	88.70	23011
3	152453	99528	260.244	349.495	89.25	24320
4	156994	80589	352.37	442.20	89.83	19842
5	152376	102323	443.50	538.16	94.66	26519
6	145973	96268	539.47	629.30	89.83	23676
7	151345	66468	630.20	719.55	89.25	16242
8	154640	84670	735.38	802.34	66.96	15522
9	150647	73856	808.52	905.93	97.41	19697

<sup>a</sup>Kepler days; convert to Julian date by adding 2454833

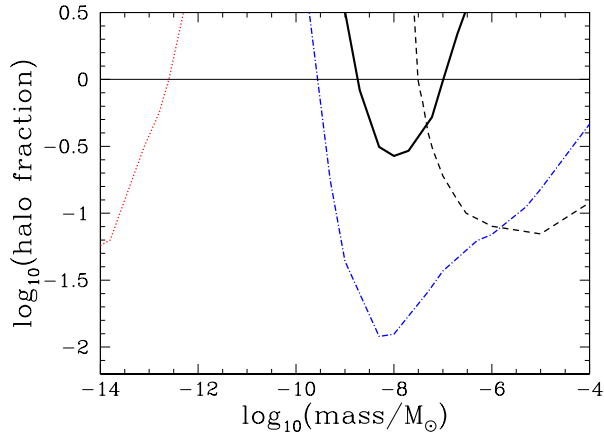


Fig. 6.— Upper limits (95% C.L.) on PBH DM from non-observation of PBH microlensing in two years of Kepler data. The solid black line is our new limit, the dashed black line is the previous best limit (Alcock, et al. (1998)), the blue dot-dash line is the theoretical limit from Paper II, and the red dotted line is the femtolensing limit from Barnacka, et al. (2012). The black horizontal line indicates a halo density of  $0.3 \text{ GeVcm}^{-3}$ .

of 8 years of data assumed in Paper II. The figure shows our experimental limits are about a factor of 8 weaker than expected. This is due to the overly optimistic efficiency assumptions made in Papers I and II. Because of the existence of many flare events, including those of short duration, we had to increase the required number of sequential high points from 4 to 5. Also non-Gaussian noise and systematic errors in the data meant we needed to add several other shape and signal-to-noise selec-

tion criteria, all of which reduced the number of microlensing events we expect to find.

Finally, the dotted red line at the left of Figure 6 shows the recent femtolensing limits from Barnacka, et al. (2012), which define the lower edge of the PBH allowed mass range. We see that there are still about 4 orders of magnitude in mass (from  $3 \times 10^{-13} M_{\odot}$  to  $2 \times 10^{-9} M_{\odot}$ ) where PBH DM (or MACHO DM) can make up the entirety of the DM. Future analysis of the entire Kepler data set should discover PBH DM or eliminate some portion of this range, and future missions such as WFIRST have the potential to cover another order of magnitude (Paper II).

K.G. and A.M.C. were supported in part by the U.S. Department of Energy under grants DE-FG03-97ER40546 and de-sc0009919. A.M.C. was supported in part by the National Science Foundation Graduate Research Fellowship under grant number DGE0707423. Some of the data presented in this paper were obtained from the Multimission Archive at the Space Telescope Science Institute (MAST). STScI is operated by the Association of Universities for Research in Astronomy, Inc., under NASA contract NAS5-26555. Support for MAST for non-HST data is provided by the NASA Office of Space Science via grant NNX09AF08G and by other grants and contracts.

## REFERENCES

- Aad, G. et al., 2012, Phys Lett. B, 716,1
- Ade, P.A.R., et al., 2013, arXiv:1303:5076
- Alcock, C., et al., 1996, Astrophys. J. **471**, 774
- Alcock, C., et al., 1998, Astrophys. J. Lett. **499**, L9
- Alcock, C., et al., 2000, Astrophys. J. **542**, 281

- Alcock, C., et al., 2001, *Astrophys. J. Lett.* **550**, L169
- ATLAS Collaboration, 2013, ATLAS-CONF-2013-001
- Barnacka, A., Glicenstein, J.F., & Moderski, R., 2012, *Phys. Rev. D*, 86, 043001
- Borucki, et al., 2010, *Science*, **327**, 977
- Carr, B.J., Kazunori, K., Sendouda, Y., & Yokoyama, J., 2010, *Phys. Rev. D* 81, 104019
- Carroll, B.W. & Ostlie, D.A., 2007, “An Introduction to Modern Astrophysics”, 2nd Edition, Appendix G, Person/Addison Wesley
- Chatrchyan, S. et al., 2013, *Phys. Lett. B*, 716, 30
- Chatrchyan, S. et al., 2012, *Phys. Rev. Lett.* 109, 171803
- Ciardi, D. R., et al., 2011, *AJ*, 141, 108
- Cieplak, A.M. & Griest, K., 2013, *ApJ*, 766, 145 (**Paper II**)
- CMS Collaboration, 2013, CMS PAS SUS-12-023; CMS PAS SUS-12-028
- Feng, J.L., 2010, *ARA&A*, 48, 495
- Frampton, P.H., et al., 2010, *JCAP* **04**, 023
- Fraquelli, D. & Thompson, S.E., 2011, *Kepler Archive Manual*, KDMC-10008-002, (<http://archive.stsci.edu/kepler>)
- Fukugita, M., et al., 1996, *AJ*, bf 111, 1748
- Griest, K., 1991, *Astrophys. J.* **366**, 412
- Griest, K., Cieplak, A.M., & Lehner, M.J., 2013, submitted.
- Griest, K., Lehner, M.J., Cieplak, A.M., & Jain, B., 2011, *Phys. Rev. Lett.* 107, 231101 (**Paper I**)
- Jungman, G., Kamionkowski, M., & Griest, K., 1996, *Phys. Rep.*, 267, 195
- Kawasaki, W., Sugiyama, N., & Yanagida, T., 1998, *Phys. Rev. D* 57, 6050
- Koch, D. G., et al. 2010, *ApJL*, 713, L79
- Khlopov, M.Y., 2008, in *Recent Advances on the Physics of compact objects and Gravitational Waves*, edited by J. A. de Freitas Pacheco
- Martin, S.P., 2011, *arXiv:hep-ph/9709356v6*
- Minor Planet Center, 2013, <http://www.minorplanetcenter.net>
- Paczynski, B., 1986, *Astrophys. J.* **304**, 1
- Sing, D.K., 2010, *A&A*. 510. A21
- Tisserand, P., et al., 2007, *Astron. & Astrophys.* **469**, 387
- Witt, H.J. & Mao, S. 1994, *ApJ*, 430, 505